Journal Pre-proofs


# High-rate GPS positioning for tracing anthropogenic seismic activity: the 29 January 2019 mining tremor in Legnica- Głogów Copper District, Poland

Iwona Kudłacik, Jan Kapłon, Grzegorz Lizurek, Mattia Crespi, Grzegorz Kurpiński

PII: S0263-2241(20)30931-3
DOI: https://doi.org/10.1016/j.measurement.2020.108396
Reference: MEASUR 108396

To appear in: *Measurement*

Received Date: 3 August 2020
Accepted Date: 24 August 2020

Please cite this article as: I. Kudłacik, J. Kapłon, G. Lizurek, M. Crespi, G. Kurpiński, High-rate GPS positioning for tracing anthropogenic seismic activity: the 29 January 2019 mining tremor in Legnica- Głogów Copper District, Poland, *Measurement* (2020), doi: https://doi.org/10.1016/j.measurement.2020.108396

# High-rate GPS positioning for tracing anthropogenic seismic activity: the 29 January 2019 mining tremor in Legnica-Głogów Copper District, Poland

Iwona Kudłacik[1,*], Jan Kapłon[1], Grzegorz Lizurek[2], Mattia Crespi[3], and Grzegorz Kurpiński[4]

[1]*Institute of Geodesy and Geoinformatics, Wrocław University of Environmental and Life Sciences, Grunwaldzka 53, Wroclaw, 50-357, Poland*

[2]*Institute of Geophysics, Polish Academy of Sciences, Księcia Janusza 64, Warszawa, 01-452, Poland*

[3]*Geodesy and Geomatics Division, DICEA-Sapienza University of Rome, via Eudossiana 18, Rome, 00184, Italy*

[4] *KGHM CUPRUM Sp. z.o.o. – Research and Development Centre, 1 Maja 14, Lubin, 59-300, Poland*

**Abstract**

High-rate GNSS observations are usually studied in relation to earthquake analysis and structural monitoring. Most of the previous research on short-term dynamic deformations has been limited to natural earthquakes with magnitudes exceeding 5 and amplitudes equal to several dozen centimetres. High-frequency position monitoring via GNSS stations is particularly important in mining areas due to the need to monitor mining damages. On 29 January 2019 (12:53:44 UTC), an M3.7 event occurred in the area of Legnica-Głogów Copper District.

This study presents GPS-derived displacement analysis in relation to seismological data. Station position time series were determined by double differencing and Precise Point Positioning. The peak ground displacement was 2–14 millimetres. The correlation coefficients between GPS and seismological displacement time series reached 0.92. A statistical evaluation of GPS displacement time series was carried out to detect an event using only GPS observations.

*Keywords:* high-rate GNSS, GNSS-seismology, mining tremor

*Corresponding author.

*Email addresses:* iwona.kudlacik@upwr.edu.pl (Iwona Kudłacik), jan.kaplon@upwr.edu.pl (Jan Kapłon), lizurek@igf.edu.pl (Grzegorz Lizurek), mattia.crespi@uniroma1.it (Mattia Crespi), g.kurpinski@cuprum.wroc.pl (Grzegorz Kurpiński)

## 1. Introduction

High-precision GNSS (Global Navigation Satellite System) observations are usually related to measurements of deformation of the earth's crust and point displacements over a long period. The standard sampling interval is usually 1–30 seconds, with the position computation in periods from several hours up to years. On the other hand, high-rate GNSS observations (HR-GNSS) refer to applications requiring high-precision positioning within a short period. The sampling frequency is in the range of 1–100 Hz and observations are processed in the kinematic mode. HR-GNSS observations are applied in natural earthquake analysis [eg. 1–9], including early warning systems [eg. 10,11], as well as structural health monitoring, e.g., dynamic behaviour of bridges [12,13].

HR-GNSS observations are usually processed using an absolute approach, such as Precise Point Positioning (PPP) [14,15], or a relative approach, such as differential positioning (DD) [16,17]. With the use of double-differencing solution, most of the systematic errors are eliminated [18]. During an earthquake, the base station might be displaced; therefore, in GNSS-seismology, the PPP approach becomes increasingly important [19]. Within short periods, up to a few minutes, high-rate PPP (HR-PPP) in kinematic mode can reach millimetre accuracy, provided convergence has been reached [20–22]. Standard PPP with a lower sampling frequency is capable of reaching positioning precisions of up to a few centimetres within tens of minutes. Shu et al. [23] analysed the influence of error sources on high-rate positioning accuracy and determined a horizontal accuracy of 3 mm and vertical of 6 mm, if ionosphere conditions do not change very rapidly within a very short time. This finding underlines that HR-PPP within a short period is significantly more accurate than conventional PPP. To perform PPP calculations, high-precision models and corrections are required, especially satellite orbits and clock corrections. Their interval and possible interpolation affect the PPP results [24–26]. Presently, the densest 5-second satellite clock corrections are provided by the Center for Orbit Determination in Europe (CODE). Lin et al. [25] concluded that the use of denser clock corrections improves positioning accuracy by smoothing the time series and reducing the noise. The alternative methodology to investigate dynamic co-seismic deformations is the variometric approach [27,28], where final products are not required, as this approach is based on broadcast orbits and the time differences of carrier phase observations from a single GNSS receiver. The GNSS sensors are significantly less sensitive for ground vibrations than seismological sensors, which results on the other hand might be potentially affected by data clipping, baseline error or mis-scaling [21,30–32].

Earthquakes can be induced by anthropogenic activities such as exploitation of water, oil and gas reservoirs, nuclear explosions or mining activity, which are called mining tremors. The Republic of Poland is located in an intraplate area where natural earthquakes are very rare. On the other hand, areas with a high density of active underground mining are threatened with induced seismicity. In Poland, these areas are mainly Upper Silesia Coal Basin (USCB) and Legnica-Głogów Copper District (LGCD) in the south, but also the open-pit mine in Bełchatów. Seismic tremors occur regularly in the underground mining areas, and there are several hundred events annually with magnitudes greater than 2, with maximum magnitudes reaching 4 [33]. As mining tremors are shallow and very frequent, they cause damage to infrastructure.

In this paper, the analysis of GPS-derived (Global Positioning System) waveforms of the first GPS-registered mining tremor with reference to seismological data is presented. The aim of this study is to examine the capacity to detect mining tremors with GPS in terms of displacements, compare the GPS-derived and seismological solutions and evaluate the detectability of mining tremors in GPS position time series. The main difference between this work and the analysis of common natural earthquakes with HR-GNSS is the event magnitude and amplitude of displacements, which here does not exceed a few centimetres, in contrast with the amplitudes reaching decimetres or even meters presented in other papers [3,8,17,34,35]. Previous studies of the application of GPS for analysis of mining effects have mostly discussed long-term displacements recorded with GNSS receivers at a rate equal or lower than 1 second [36–40], often in integration with InSAR technology [eg. 41].

## 2. Data

Since the launch of the high-rate GNSS network through the efforts of the EPOS-PL project and the University of Warmia and Mazury in Olsztyn, the most prominent mining tremor event that has been recorded was in the area of LGCD on 29 January 2019 (12:53:44 UTC), with a magnitude of 3.7. The epicentre was located at 51.51°N, 16.12°E, with a hypocentral depth of 800 m, a source radius of over 300 m and a cavity collapse mechanism, provided by the Institute of Geophysics, Polish Academy of Sciences. Three high-rate GNSS stations, close to seismic stations (SM), were located within approx. 3 km of the epicentre; a map of the co-located stations is shown in Figure 1. The distances between co-located GNSS and seismic stations and their epicentral distances are listed in Table 1.

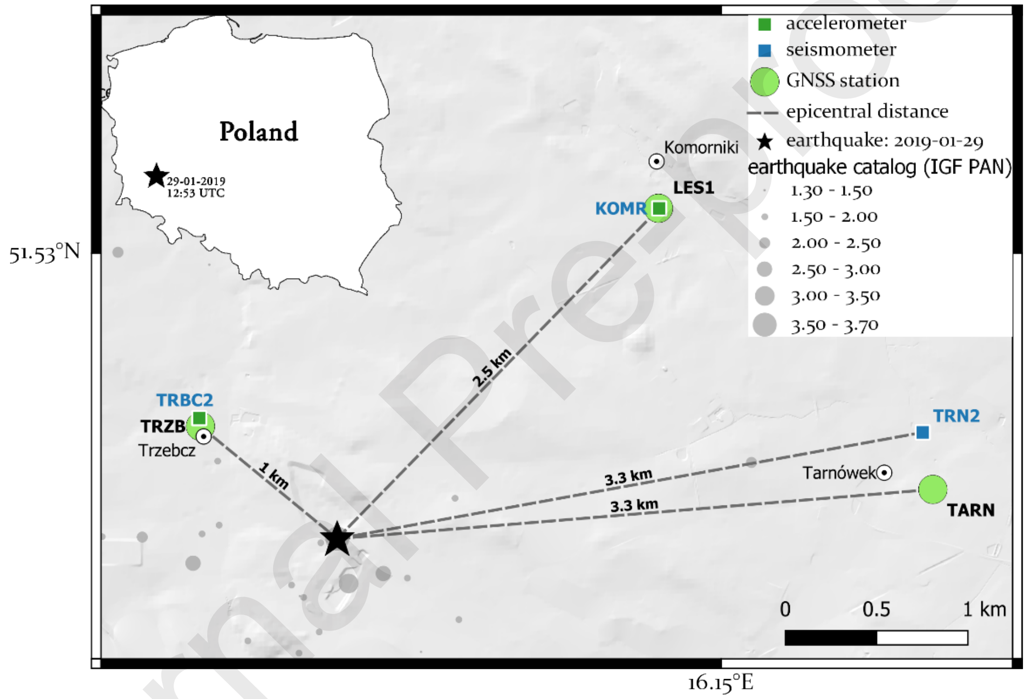


Figure 1: Distribution of the high-rate GNSS stations (green circles) and the seismic stations (squares) in the proximity of the 2019 mining tremor. The black star is the epicentre location. The data from the earthquake catalogue refer to the period from July 2018 to March 2019.

Table 1: Details of co-located high-rate GNSS and strong-motion stations.

| GNSS/SM | ORIGINAL GNSS/SM SAMPLING | SM TYPE | ORIGINAL GNSS DATA | SEPARATION [KM] | EPICENTRAL DISTANCE [KM] |
|---|---|---|---|---|---|
| **LES1/KOMR** | 10 Hz/250Hz | accelerometer | GPS, Galileo, GLONASS, BDS, QZSS, SBAS | 0.002 | 2.523 |
| **TRZB/TRBC2** | 50 Hz/250 Hz | accelerometer | GPS, Galileo | 0.045 | 1.000 |
| **TARN/TRN2** | 50 Hz/100 Hz | seismometer | GPS | 0.316 | 3.267 |

# 3. Methods

## 3.1. Seismological data preparation

Concerning seismological data, accelerations and velocities were integrated into displacements (denoted as SM-displacements), and the timestamps were transformed into the GPS time. Then, the displacement time series were high-pass filtered with a cut-off frequency of 0.015 Hz to remove the low frequencies remaining from numerical integration and decimated to 10 Hz to perform consistency analysis of the GPS- and SM-time series.

## 3.2. GPS-data processing

In this study, the GPS position time series were obtained from phase measurements in the kinematic mode with two approaches: Precise Point Positioning (PPP) and relative differential positioning (DD). The accuracy of both PPP and DD approaches in short periods is similar. The influence of potential errors, induced by atmosphere or tectonics, are minor, in contrast to long-term positioning. In contrast to large natural earthquakes, short term ground vibrations occurring during the mining tremors are detectable with GNSS observations only on small areas. Therefore, the problem of the potential instability of the reference station does not exist. However, the closest reference station with corresponding sampling frequency often might be localised in the long-distance from the mining area, to not be exposed to long-term mining deformations. In both solutions – PPP and DD, two-hour-long 10 Hz GPS observations were processed. We decided to attenuate the sampling frequency of the TRZB and TARN stations to 10 Hz; the original 50-Hz observations resulted in higher noise values, and for this event, such a high sampling frequency is irrelevant, as the spectral window of vibrations does not exceed 2.5 Hz. DD solution was obtained with GAMIT software [16] using the CODE Final GPS orbit and clock products, with the UQRG high-resolution global ionosphere model from UPC [42]. We used the Melbourne-Wűbbena (L6) linear combination of L1 and L2 GPS frequencies to process the long baseline with ambiguity resolution, providing the satellite and receiver clock error mitigation and reference for the high-rate positioning from outside the mining region. The reference station, WROE, is located 79 km south-east of the epicentre, as presented in Figure 1. The PPP solution was obtained using the same precise final ephemerides as for the DD solution and 5-sec clock data from the Centre of Orbit Determination in Europe (CODE) with RTKlib v2.4.3 software [43]. To validate the accuracy of the PPP solutions performed with RTKlib, the GPS dataset was calculated with the online CSRS-PPP application (the Canadian Spatial Reference System Precise Point Positioning tool), where IGS clock and orbit products are used, and the troposphere delay is calculated with Global Mapping Function. The PPP solution was performed without estimating integer ambiguities. The position time series were obtained in geocentric Cartesian coordinates (XYZ) and then transformed to the local topocentric Cartesian coordinates and to relative positions (denoted as GPS-displacements).

To estimate amplitudes and compare the GPS time series with seismological data, the time series needed to be reduced to one spectral window where both types of instruments registered the earthquake. This was done by applying the 2nd-order Butterworth band-pass filter. To prevent filtering the seismologically important frequencies, the Fourier spectra of displacement time series of co-located seismic sensors were analysed (first row in Figure 2) and the cut-of frequencies were determined on this basis. For all three sets of co-located stations, the high-pass cut-off frequency was set to 0.15 Hz. The analysis of high-frequency noise resulted in the selection of two values for the low-pass cut-off frequency. Due to the different ground characteristics of the TARN station, for this station, the spectral window needed to be limited to 0.15–1.20 Hz, while for the other two stations, it was set to 0.15–2.00 Hz. The dominant frequencies of the DD and PPP approaches are consistent, which agrees with the results presented by [34] for the very large natural earthquake.

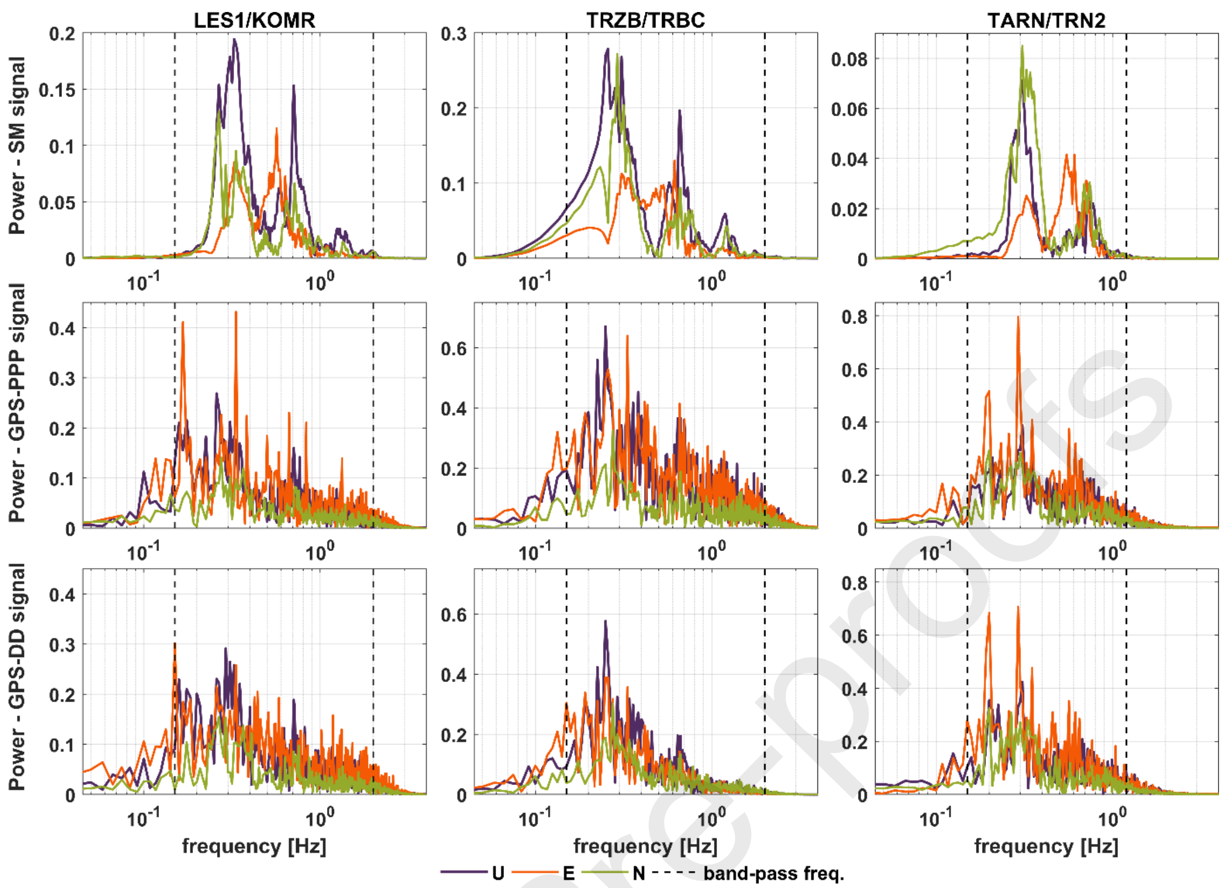


Figure 2: Fourier spectra of band-pass filtered displacement waveforms.

The accuracy of the GPS-positions obtained with the CSRS-PPP, RTKlib-PPP and GAMIT-DD approaches are listed in Table 2. The accuracy was determined as the unbiased version of RMSE over 2-minute windows averaged during 60-minute time-series in stable conditions before an analysed mining tremor. They were calculated for non-filtered positions with the linear trend removed and for band-pass filtered positions. In particular, the RTKlib-PPP solutions show a significant linear trend, which had to be removed for further analysis. For non-filtered positions over 2-minutes, the accuracy is several millimetres, up to over 1 centimetre for the vertical component. The accuracy after band-pass filtering is comparable between all solutions, the error is over 65% smaller than for non-filtered GPS-positions, approximately 2 mm for the horizontal component and 4 mm for the vertical. Since the filtered CSRS-PPP and RTKlib-PPP solutions are consistent, for further analysis, the RTKlib-PPP results were used. The application of Butterworth filter led to reducing the low-frequency fluctuations, which for PPP solutions are probably caused by some unmodelled errors and for DD solution by some ionosphere error left due to long baseline.

Table 2: Accuracy of non-filtered (linear detrended) and band-pass filtered GPS-positions in stable conditions. The accuracy was determined as the unbiased version of RMSE. The time span is 2 minutes.

| APPROACH | STATION | NON-FILTERED | | | SPECTRAL WINDOW [HZ] | BAND-PASS FILTERED | | |
|---|---|---|---|---|---|---|---|---|
| | | E [MM] | N [MM] | U [MM] | | E [MM] | N [MM] | U [MM] |
| **RTKLIB-PPP** | LES1 | 2.4 | 3.5 | 7.9 | 0.15–2.00 | 0.6 | 1.0 | 1.9 |
| **CSRS-PPP** | LES1 | 3.3 | 6.5 | 9.7 | 0.15–2.00 | 0.6 | 1.0 | 2.0 |
| **GAMIT-DD** | LES1 | 2.5 | 6.5 | 14.6 | 0.15–2.00 | 0.8 | 1.8 | 2.1 |
| **RTKLIB-PPP** | TRZB | 4.6 | 5.5 | 12.0 | 0.15–2.00 | 2.0 | 2.7 | 5.8 |
| **CSRS-PPP** | TRZB | 3.9 | 6.5 | 12.2 | 0.15–2.00 | 1.3 | 2.0 | 3.9 |
| **GAMIT-DD** | TRZB | 3.7 | 6.0 | 18.5 | 0.15–2.00 | 0.7 | 1.1 | 1.0 |
| **RTKLIB-PPP** | TARN | 3.0 | 5.6 | 13.5 | 0.15–1.20 | 2.3 | 3.6 | 4.5 |
| **CSRS-PPP** | TARN | 3.7 | 5.9 | 9.5 | 0.15–1.20 | 1.5 | 2.3 | 4.7 |
| **GAMIT-DD** | TARN | 4.4 | 5.6 | 9.1 | 0.15–1.20 | 2.1 | 2.9 | 6.5 |

### 3.3. Time series analysis

Considering the event length, for further analysis GPS- and SM-displacement time series were reduced to the period starting 30 sec before an event and finishing 90 sec after.

First, both time series were compared in terms of the Peak Ground Displacement (PGD), defined as the maximum absolute value of the 3D waveform, and the peak-to-peak amplitude (AMPLITUDE), defined as the maximum difference between peaks. Next, the Root Mean Square Error (RMSE) was determined, taking the SM-displacement time series as a reference. These three coefficients were calculated for the band-pass filtered GPS-displacement time series.

The next step of the similarity analysis was to perform coherence analysis in the frequency domain [19,44]. The magnitude square coherence was determined using Welch's overlapped averaged periodogram method, provided by Matlab. A Hamming window of 100 samples (10 seconds) and 80 samples of overlapping were used. In the literature, two time series are usually assumed to be strongly correlated in the frequency domain if coherence exceeds 0.8 [45]. Then, the Pearson's correlation coefficient was calculated, and the time variability analysis of standard deviation (STD), median absolute deviation (MAD), mean and median of the GPS-displacement time series were calculated. The STD and MAD were calculated, assuming that during the period of analysis the station would be stable, if an event would not occur. We used MAD, as it is a robust statistic, in contrast with STD, which is strongly influenced by outliers [46,47]. All aforementioned coefficients were analysed within a 10-sec moving window and were used to test the ability to detect mining tremor with GPS-displacement time series only. The 10-sec window length was chosen on the basis of an event length, considering the number of samples in this period [27].

## 4. Results and discussion

### 4.1. Comparison of GPS- and SM-displacements

The peak ground displacements (PGDs) calculated for stations LES1 and TRZB with the PPP-approach were very close to the PGDs calculated with the seismological data co-located with the GNSS stations (Table 3). For these two stations, the results obtained with the DD approach appear to be underestimated in comparison with the seismological data and PPP displacements. In both approaches, the PGD of the TARN station is significantly larger than for the co-located TRN2 station, the difference is mainly due to the 316 m separation between sensors. For this pair of sensors, there are also significant differences in amplitude values.

The RMSE reached about 1-1.5 mm for station LES1, which confirms the consistency between the displacement time-series of the very closely co-located stations LES1 and KOMR in both approaches. For stations TRZB and TARN, the RMSE values were twice as large, which is likely the result of amplitude difference, higher noise level and greater separation between sensors.

Table 3: Peak ground displacements, peak-to-peak amplitudes and RMSE of filtered PPP and DD displacements (mm).

| APPROACH | GPS/SM STATION | SEPARATION [KM] | PGD | | AMPLITUDE (GPS) | | | AMPLITUDE (SM) | | | RMSE | | |
|---|---|---|---|---|---|---|---|---|---|---|---|---|---|
| | | | GPS | SM | E | N | U | E | N | U | E | N | U |
| **PPP** | LES1/KOMR | 0.002 | 9.0 | 9.0 | 6.6 | 15.0 | 11.1 | 5.5 | 14.8 | 8.8 | 0.5 | 1.0 | 1.3 |
| **PPP** | TRZB/TRBC2 | 0.045 | 14.9 | 14.5 | 18.5 | 31.3 | 22.7 | 14.3 | 23.7 | 11.5 | 2.1 | 4.2 | 4.6 |
| **PPP** | TARN/TRN2 | 0.316 | 8.5 | 2.2 | 11.7 | 11.0 | 16.6 | 4.1 | 2.8 | 2.8 | 1.3 | 1.7 | 2.3 |
| **DD** | LES1/KOMR | 0.002 | 8.8 | 9.0 | 7.8 | 15.0 | 14.1 | 5.5 | 14.8 | 8.8 | 0.6 | 1.2 | 1.4 |
| **DD** | TRZB/TRBC2 | 0.045 | 8.1 | 14.5 | 12.8 | 15.9 | 10.8 | 14.3 | 23.7 | 11.5 | 0.8 | 1.8 | 1.8 |
| **DD** | TARN/TRN2 | 0.316 | 8.5 | 2.2 | 12.6 | 11.4 | 16.6 | 4.1 | 2.8 | 2.8 | 1.3 | 1.8 | 2.4 |

### 4.2. Time series consistency

The consistency of the GPS- and SM-displacement time series in the frequency domain was assessed using coherence analysis in the common frequency range of 0–5 Hz. The PPP-processed displacement time series coherence values were similar to those for the DD-processed data (Figure 3). According to the literature, a statistically significant coherence value should exceed 0.8. However, in the case of this mining tremor, which was relatively small compared to other studies concerning GPS seismology [3,5,17], the signal-to-noise ratio is smaller. Thus, in the performed coherence analysis, most of the visible coherence peaks are not statistically significant (Figure 3). Therefore, the frequencies where coherence was greater than 0.6 were marked as significant; these probably represent the earthquake dominant frequencies. For all three sets of stations, the coherence values were comparable between the two approaches, especially for the less noiser horizontal components, where there were two significant peaks of coherence values at frequencies 0.31–0.39 and 0.66–0.74 Hz. The vertical component, usually much noiser, has slightly different characteristics, and there was no significant peak for station TRZB, whereas for the other two stations (LES1 and TARN), there was a peak of coherence values at frequencies 0.47–0.55 Hz.

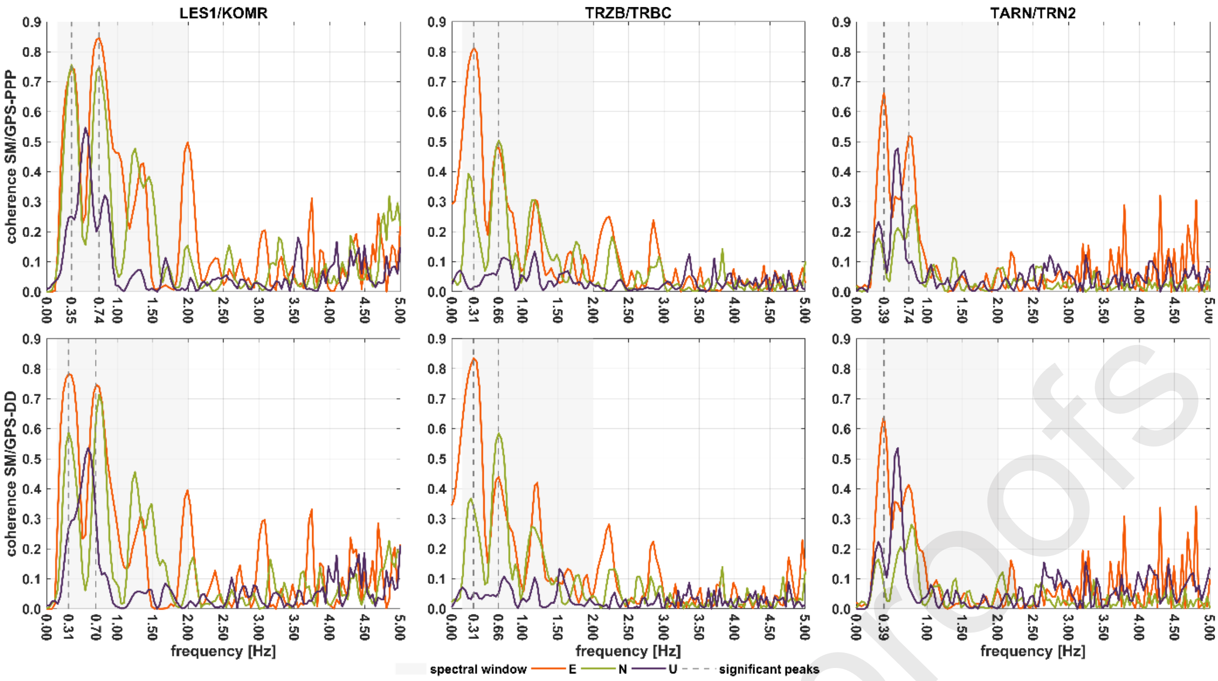


Figure 3: Coherence values of band-pass filtered displacements calculated with the PPP (top) and DD (bottom) approaches.

Next, the Pearson's correlation coefficients of the GPS- and SM-displacement time series were compared. In stable conditions, when no earthquake occurs, it is assumed that GPS- and SM-displacement time series should not be correlated and any increase in the correlation coefficient is random. However, during an event, the correlation should significantly increase. To assess this hypothesis, the time variability of Pearson's correlation coefficient was examined with a 10-second moving window. The results, presented in Figures 4–5, confirm the increase of the correlation during an earthquake. However, when the noise level is comparable with the earthquake amplitude, random jumps in the correlation coefficient occur, as for station TARN, presented in Figure 5b. Moreover, the correlation coefficient depends on noise level and the clarity of an event in the data; therefore, for the TARN and TRZB stations (Figure 5), the correlation coefficients are significantly lower than for the LES1 station (Figure 4). The maximum correlation coefficients obtained during an earthquake are listed in Table 4. The values strongly depend on the separation between sensors and the noise level of the GPS displacement time series.

Table 4: List of maximum correlation coefficients for PPP/SM and DD/SM band-pass filtered displacement time series.

| *STATION* | *SEPARATION [km]* | *SPECTRAL WINDOW [Hz]* | *DD/SM* | | | *PPP/SM* | | |
|---|---|---|---|---|---|---|---|---|
| | | | **E** | **N** | **U** | **E** | **N** | **U** |
| ***LES1*** | **0.002** | **0.15–2.00** | 0.93 | 0.89 | 0.87 | 0.92 | 0.92 | 0.84 |
| ***TRZB*** | **0.045** | **0.15–2.00** | 0.94 | 0.89 | 0.52 | 0.90 | 0.82 | 0.58 |
| ***TARN*** | **0.316** | **0.15–1.20** | 0.66 | 0.55 | 0.70 | 0.70 | 0.61 | 0.62 |

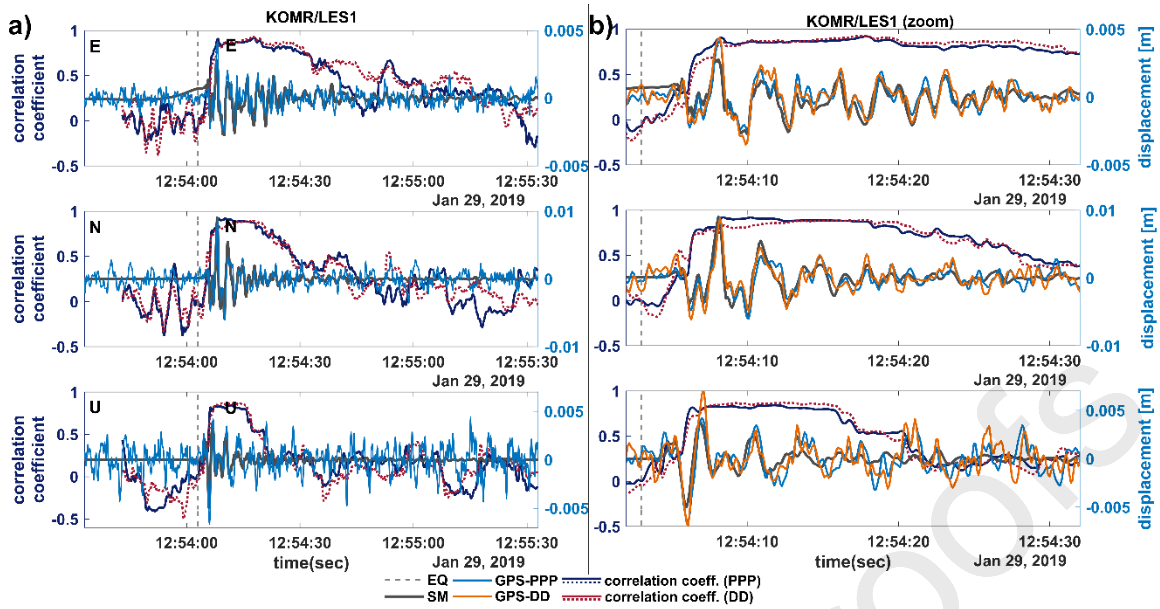


Figure 4: Time variability of Pearson's correlation coefficient of band-pass filtered displacements in comparison with seismological data for station KOMR/LES1. Left panel "a" presents 2-minute time series of SM and PPP-displacements. Right panel "b" presents 30-second time series of SM, PPP and DD-displacements. On both panels, the correlation coefficient variability for both solutions is presented.

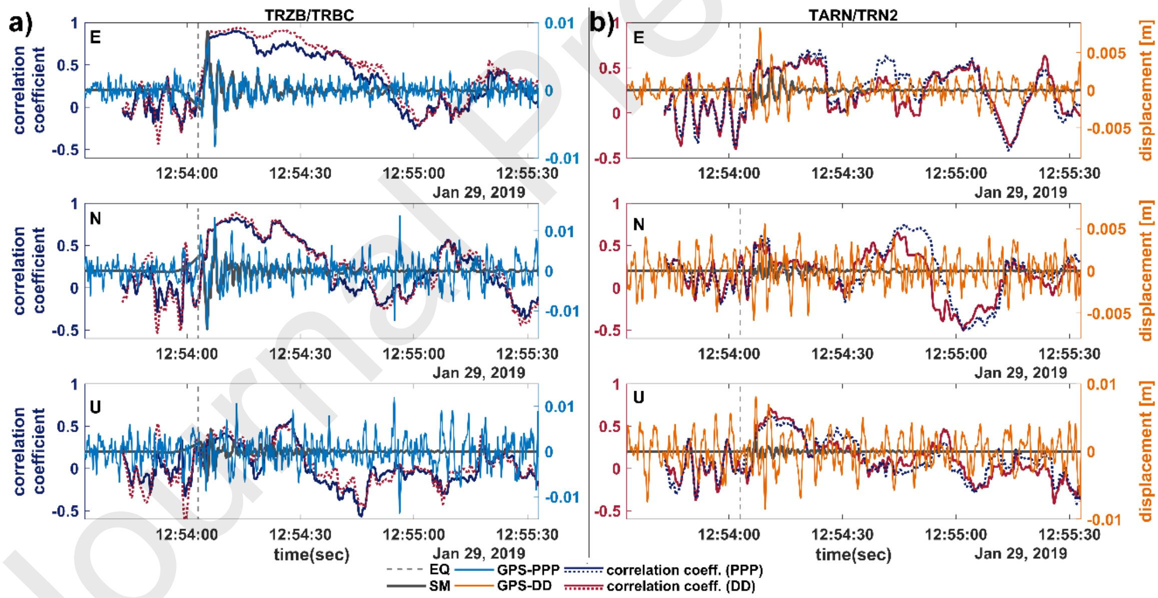


Figure 5: Time variability of Pearson's correlation coefficient of band-pass filtered displacements in comparison with seismological data on 2-minute time series. Left panel "a" presents PPP-displacements for station TRZB/TRBC and right panel "b" presents DD-displacements for station TARN/TRN2. On both panels, the correlation coefficient variability for both solutions is presented.

## 4.3. Detection of mining tremor in GPS position time series

As GNSS stations dedicated to dynamic displacement monitoring are not always co-located with seismological instruments, we decided to test the mining tremor detection performance of GPS-displacement alone using statistical evaluations. Hence, we tested the time variability of mean, median, standard deviation and median absolute deviation in a 10-second moving window, shifting every epoch. The test was performed for PPP and DD processing approaches with band-pass filtering.

It has been presented that the low frequencies are eliminated by filtering since the median and mean coincide and oscillate around zero. The standard deviation (STD) and median absolute deviation (MAD) in stable conditions within a 10-second window oscillate around the values listed in Table 2. However, once the tremor occurs, both coefficients rapidly increase, reaching their maximum value when the window covers the entire event, which is especially clear for the horizontal component. After an event, STD and MAD return to the values present in stable conditions. As MAD is more robust to outliers than STD, the increase is less prompt and it requires more event samples to occur.

The clarity of the increases in MAD and STD during the tremor depends strongly on the noise level of the time series. The comparison of STD and MAD on the band-pass filtered displacement time series revealed the higher significance of the horizontal components in all tested cases, since they are less noiser. The tremor is clearest in STD and MAD for the displacements calculated with the DD approach, as in DD displacement time series, random jumps of these coefficients do not occur. From the analysed stations, in both approaches, the best result was revealed for the LES1 station (Figure 6), where the noise level is the lowest. The changes in STD and MAD are clearly visible for the East and North components of LES1 PPP-displacements, where both coefficients increase from values of approx. 0.4 and 1 mm to 1.5 and 2.6 mm, respectively. Interestingly, the displacement time series in the East direction is more stable than that in the North direction. For the vertical component, the increases in MAD and STD during the mining tremor were not clear. The aforementioned results were also observed for the other two stations, TRZB and TARN, but the changes in MAD and STD were even less noticeable. However, for all three stations, the change was definitely the clearest in the East displacement time series.

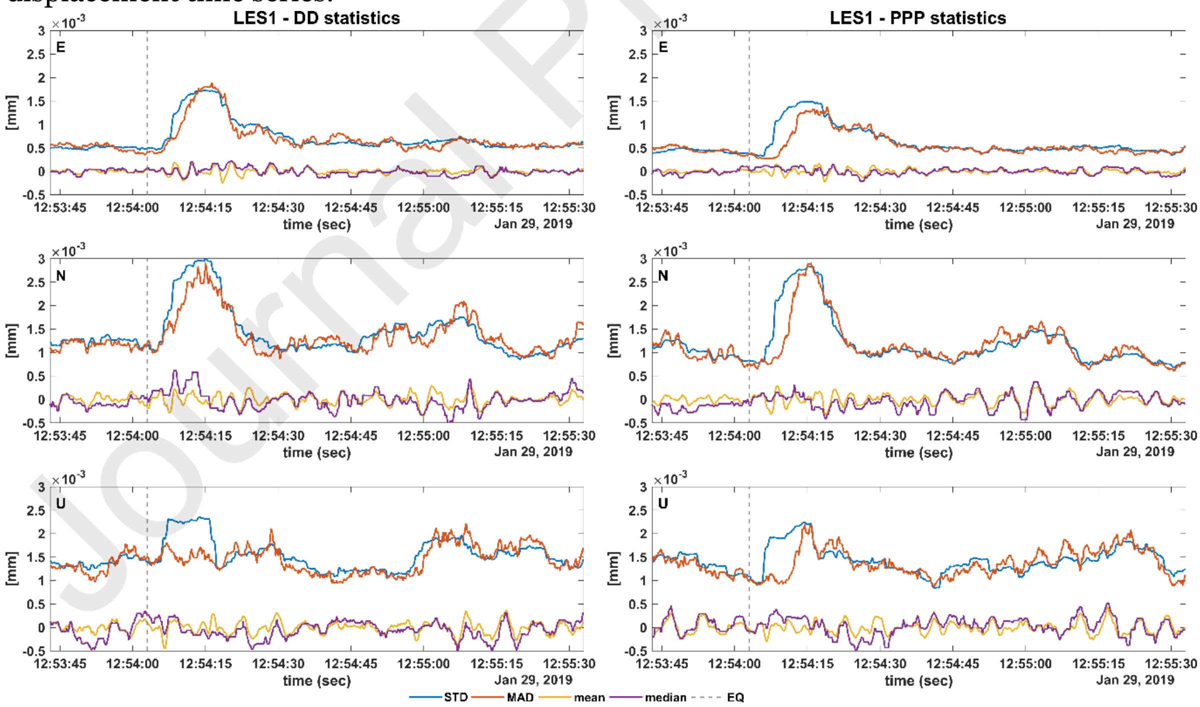


Figure 6: Statistics for the station LES1 2-minute band-pass filtered displacement time series calculated with the PPP (right) and DD approaches (left).

To determine that the increases in STD and MAD were not coincidental, it was decided to evaluate the changes in STD and MAD over a one-hour period for the East and North displacements transformed into horizontal displacements. This analysis revealed that with the PPP approach, for the LES1 displacement time series, the increases in STD and MAD for the horizontal component are essential and make it possible to identify this event (Figure 7). For the PPP-processed TARN and TRZB displacements, however, the values of STD and MAD were high and varying; therefore, the change observed during the event was not distinct enough to identify the occurrence of the mining tremor using the GPS time series alone. With the DD approach, the event is detectable using STD and MAD for both the LES1 and TRZB stations. The example of station TRZB is presented in Figure 8. Unfortunately, for the TARN station, the tremor is not clearly visible in the STD and MAD changes.

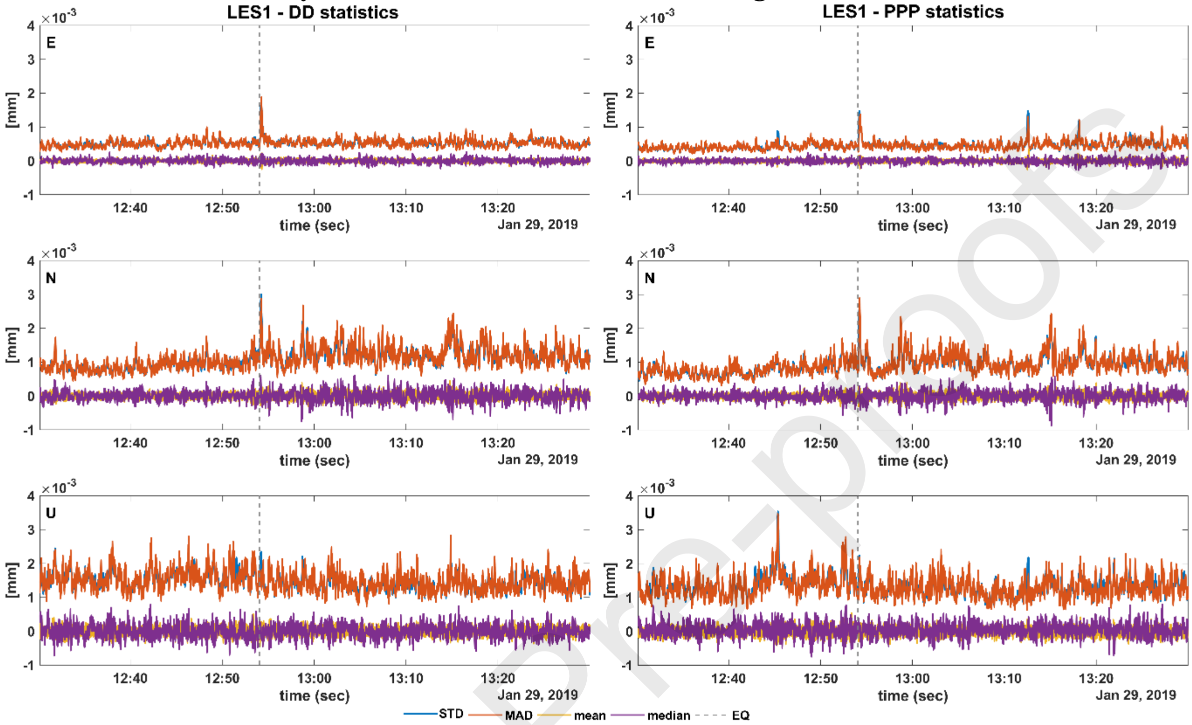


Figure 7: Statistics for the LES1 1-hour band-pass filtered displacement time series calculated with the PPP (right) and DD approaches (left).

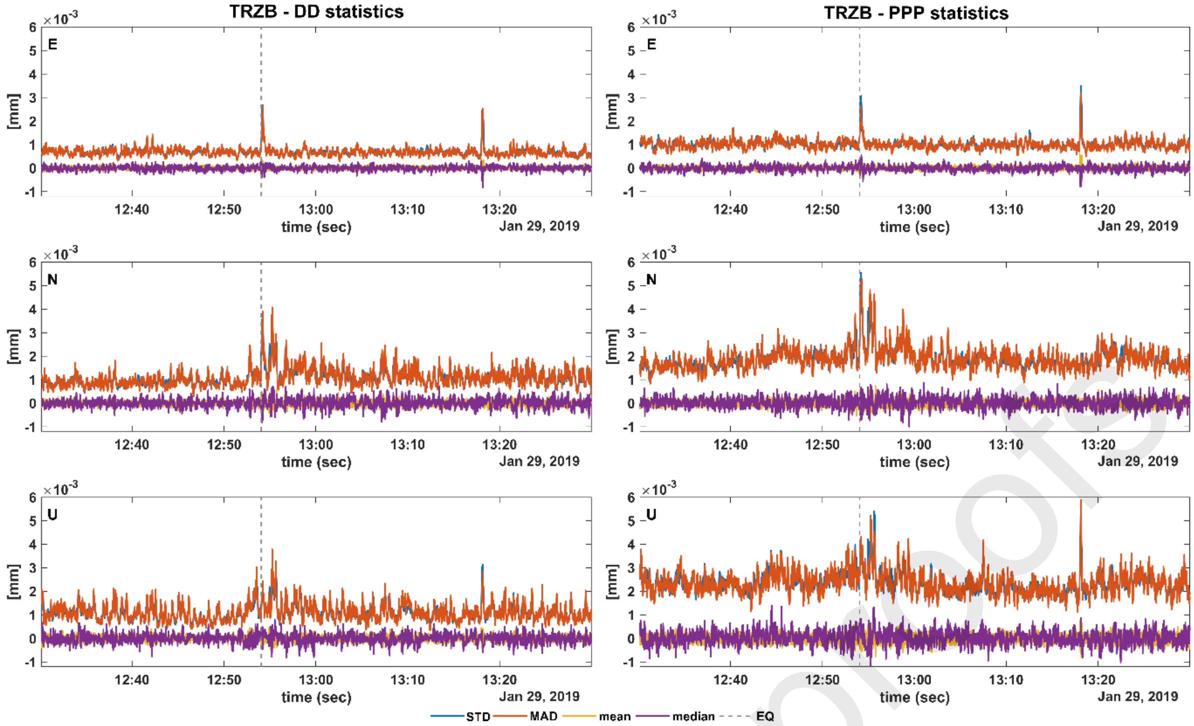


Figure 8: Statistics for the TRZB 1-hour band-pass filtered displacement time series calculated with the PPP (right) and DD approaches (left).

## 5. Conclusions

In conclusion, to the best of our knowledge, this is the first study to analyse mining tremor using the high-rate GNSS technique, here limited to GPS data. Other studies have concerned natural earthquake analysis with HR-GNSS, and if they addressed induced shocks, it was only in the area of long-term displacement and standard sampling frequencies of up to 1 Hz. In the case of the Legnica-Głogów Copper District mining tremor, the peak ground displacements reached 16 mm and the comparison between GPS and SM derived displacements exhibited a Pearson's correlation value ranging from 0.61 to 0.94 for horizontal displacements, after band-pass filtering to remove low-frequency trends and high frequency noise. In this study, second order Butterworth band-pass filtering was applied. For the DD results, high-pass filtering is sufficient to obtain good agreement with seismological displacements, whereas for the PPP results, reduction of high-frequency noise is also important. The agreement in terms of coherence is significant for the dominant frequencies for this event, which are in the range of 0.3–0.7 Hz. The results of detection tests showed that it is possible to detect a mining tremor with a GPS displacement time series alone. The changes in standard deviation and median absolute deviation associated with such a tremor are detectable, especially for a horizontal displacement time series calculated with the DD approach.

These results indicate that not only natural earthquakes of magnitudes over 5 can be analysed with GNSS technique, but smaller events might also be recorded with GPS receivers when the epicentral distance is shorter, benefiting of its high resistance to saturation. This method might be supplementary in seismological analysis, provided that the noise is minimized, for example, with digital filtering. Moreover, the GPS results might validate the orientation of seismological instruments, which is crucial in epicentre localization.

In mining areas, a dense network of low-cost GNSS receivers recording with a minimum frequency of 5 Hz would allow for more extensive analysis of post-mining ground deformations and could contribute to more accurate determination of event parameters.

## 6. Declaration of interests

The authors declare that they have no known competing financial interests or personal relationships that could have appeared to influence the work reported in this paper.

## 7. Acknowledgements

This work was carried out within EPOS – the European Plate Observing System, co-financed by the European Union from the funds of the European Regional Development Fund, POIR.04.02.00-14-A0003/16. Seismological data for this study was provided by the Institute of Geophysics, Polish Academy of Sciences and are available in https://tcs.ah-epos.eu/#episode:LGCD. The GNSS data from the TRZB and TARN stations was provided courtesy of KGHM Cuprum Sp. z. o. o. and the University of Warmia and Mazury, co-financed by the National Centre for Research and Development, POIR.04.01.04-00-0056/17. The authors thank these institutions for their kind help. Grzegorz Lizurek was partially supported by statutory activities No. 3841/E-41/S/2020 of the Ministry of Science and Higher Education of Poland. This work has been supported by the Wroclaw Center of Networking and Supercomputing (http://www.wcss.wroc.pl): computational grant using MATLAB Software License No. 101979. The authors are glad to recognize that the anonymous Reviewers' comments remarkably contributed to improve the manuscript.

## 8. References

[1] X. Li, K. Zheng, X. Li, G. Liu, M. Ge, J. Wickert, H. Schuh, Real-time capturing of seismic waveforms using high-rate BDS, GPS and GLONASS observations: the 2017 Mw 6.5 Jiuzhaigou earthquake in China, GPS Solut. 23 (2019) 17. https://doi.org/10.1007/s10291-018-0808-9.

[2] I. Kudlacik, J. Kapłon, J. Bosy, G. Lizurek, Seismic phenomena in the light high-rate GPS precise point positioning results, Acta Geodyn. Geomater. 193 (2019) 99–112. https://doi.org/10.13168/AGG.2019.0008.

[3] Y. Shu, R. Fang, J. Geng, Q. Zhao, J. Liu, Broadband Velocities and Displacements From Integrated GPS and Accelerometer Data for High-Rate Seismogeodesy, Geophys. Res. Lett. 45 (2018) 8939–8948. https://doi.org/10.1029/2018GL079425.

[4] H.K. Hung, R.J. Rau, E. Benedetti, M. Branzanti, A. Mazzoni, G. Colosimo, M. Crespi, GPS Seismology for a moderate magnitude earthquake: Lessons learned from the analysis of the 31 October 2013 ML6.4 Ruisui (Taiwan) earthquake, Ann. Geophys. 60 (2017). https://doi.org/10.4401/ag-7399.

[5] C. Michel, K. Kelevitz, N. Houlié, B. Edwards, P. Psimoulis, Z. Su, J. Clinton, D. Giardini, The potential of high-rate GPS for strong ground motion assessment, Bull. Seismol. Soc. Am. 107 (2017) 1849–1859. https://doi.org/10.1785/0120160296.

[6] S. Häberling, M. Rothacher, Y. Zhang, J.F. Clinton, A. Geiger, Assessment of high-rate GPS using a single-axis shake table, J. Geod. 89 (2015) 697–709. https://doi.org/10.1007/s00190-015-0808-2.

[7] E. Benedetti, M. Branzanti, L. Biagi, G. Colosimo, A. Mazzoni, M. Crespi, Global navigation satellite systems seismology for the 2012 Mw 6.1 emilia earthquake: Exploiting the vadase algorithm, Seismol. Res. Lett. 85 (2014) 649–656. https://doi.org/10.1785/0220130094.

[8] M. Branzanti, G. Colosimo, M. Crespi, A. Mazzoni, GPS near-real-time coseismic displacements for the great Tohoku-Oki earthquake, IEEE Geosci. Remote Sens. Lett. 10 (2013) 372–376. https://doi.org/10.1109/LGRS.2012.2207704.

[9] K.M. Larson, P. Bodin, J. Gomberg, Using 1-Hz GPS data to measure deformations caused by the denali fault earthquake, Science (80-. ). 300 (2003) 1421–1424. https://doi.org/10.1126/science.1084531.

[10] P.A. Psimoulis, N. Houlié, M. Habboub, C. Michel, M. Rothacher, Detection of ground motions using high-rate GPS time-series, Geophys. J. Int. 214 (2018) 1237–1251. https://doi.org/10.1093/gji/ggy198.

[11] P.A. Psimoulis, N. Houlié, Y. Behr, Real-Time Magnitude Characterization of Large Earthquakes Using the Predominant Period Derived From 1 Hz GPS Data, Geophys. Res. Lett. 45 (2018) 517–526. https://doi.org/10.1002/2017GL075816.

[12] M.R. Kaloop, C.O. Yigit, A.A. Dindar, M. Elsharawy, J.W. Hu, Evaluation of the high-rate GNSS-PPP method for vertical structural motion, Surv. Rev. (2018) 1–13. https://doi.org/10.1080/00396265.2018.1534362.

[13] C.O. Yigit, E. Gurlek, Experimental testing of high-rate GNSS precise point positioning (PPP) method for detecting dynamic vertical displacement response of engineering structures, Geomatics, Nat. Hazards Risk. 0 (2017) 1–12. https://doi.org/10.1080/19475705.2017.1284160.

[14] J.F. Zumberge, M.B. Heflin, D.C. Jefferson, M.M. Watkins, F.H. Webb, Precise point positioning for the efficient and robust analysis of GPS data from large networks, J. Geophys. Res. Solid Earth. 102 (1997) 5005–5017. https://doi.org/10.1029/96JB03860.

[15] P. Xu, Y. Shu, J. Liu, T. Nishimura, Y. Shi, J.T. Freymueller, A large scale of apparent sudden movements in Japan detected by high-rate GPS after the 2011 Tohoku Mw9.0 earthquake: Physical signals or unidentified artifacts?, Earth, Planets Sp. 71 (2019). https://doi.org/10.1186/s40623-019-1023-9.

[16] T.A. Herring, R.W. King, M.A. Floyd, S. McClusky, GAMIT reference manual, release 10.7, Massachusetts Inst. Technol. Cambridge. (2018).

[17] A. Avallone, D. Latorre, E. Serpelloni, A. Cavaliere, A. Herrero, G. Cecere, N. D'Agostino, C. D'Ambrosio, R. Devoti, R. Giuliani, M. Mattone, S. Calcaterra, P. Gambino, L. Abruzzese, V. Cardinale, A. Castagnozzi, G. De Luca, L. Falco, A. Massucci, A. Memmolo, F. Migliari, F. Minichiello, R. Moschillo, L. Zarrilli, G. Selvaggi, Coseismic displacement waveforms for the 2016 August 24 Mw 6.0 Amatrice earthquake (central Italy) carried out from high-rate GPS data, Ann. Geophys. 59 (2016) 1–11. https://doi.org/10.4401/ag-7275.

[18] R.S. Nerem, K.M. Larson, Global positioning system, theory and practice, 5th edition, 2001. https://doi.org/10.1029/01e000224.

[19] P. Psimoulis, N. Houlié, M. Meindl, M. Rothacher, Consistency of PPP GPS and strong-motion records: Case study of Mw9.0 Tohoku-Oki 2011 earthquake, Smart Struct. Syst. 16 (2015) 347–366. https://doi.org/10.12989/sss.2015.16.2.347.

[20] J. Hefty, L. Gerhátová, Potential of precise point positioning using 1 HZ GPS data for detection of seismic-related displacements, Acta Geodyn. Geomater. 9 (2012) 303–313.

[21] P. Xu, C. Shi, R. Fang, J. Liu, X. Niu, Q. Zhang, T. Yanagidani, High-rate precise point positioning (PPP) to measure seismic wave motions: An experimental comparison of GPS PPP with inertial measurement units, J. Geod. 87 (2013) 361–372. https://doi.org/10.1007/s00190-012-0606-z.

[22] J. Geng, Y. Pan, X. Li, J. Guo, J. Liu, X. Chen, Y. Zhang, Noise Characteristics of High-Rate Multi-GNSS for Subdaily Crustal Deformation Monitoring, J. Geophys. Res. Solid

Earth. 123 (2018) 1987–2002. https://doi.org/10.1002/2018JB015527.

[23] Y. Shu, Y. Shi, P. Xu, X. Niu, J. Liu, Error analysis of high-rate GNSS precise point positioning for seismic wave measurement, Adv. Sp. Res. 59 (2017) 2691–2713. https://doi.org/10.1016/j.asr.2017.02.006.

[24] A. Hesselbarth, L. Wanninger, Short-term stability of GNSS satellite clocks and its effects on precise point positioning, in: Proc. ION GNSS, 2008: pp. 1855–1863.

[25] X. Lin, F. Guo, C. Lv, Y. Xu, Impacts of sampling rates of IGS satellite clock on convergence of precise point positioning, Wuhan Daxue Xuebao (Xinxi Kexue Ban)/Geomatics Inf. Sci. Wuhan Univ. 35 (2010) 683–686.

[26] M. Szołucha, K. Kroszczyński, D. Kiliszek, Accuracy of Precise Point Positioning (PPP) with the use of different International GNSS Service (IGS) products and stochastic modelling, Geod. Cartogr. 67 (2018) 207–238. https://doi.org/10.24425/gac.2018.125472.

[27] G. Colosimo, M. Crespi, A. Mazzoni, Real-time GPS seismology with a stand-alone receiver: A preliminary feasibility demonstration, J. Geophys. Res. Solid Earth. 116 (2011). https://doi.org/10.1029/2010JB007941.

[28] E. Benedetti, M. Branzanti, G. Colosimo, A. Mazzoni, M. Crespi, VADASE: State of the art and new developments of a third way to GNSS seismology, in: Int. Assoc. Geod. Symp., 2016: pp. 59–66. https://doi.org/10.1007/1345_2015_7.

[29] A. Bilich, J.F. Cassidy, K.M. Larson, GPS seismology: Application to the 2002 Mw 7.9 Denali fault earthquake, Bull. Seismol. Soc. Am. 98 (2008) 593–606. https://doi.org/10.1785/0120070096.

[30] D.M. Boore, Effect of baseline corrections on displacements and response spectra for several recordings of the 1999 Chi-Chi, Taiwan, earthquake, Bull. Seismol. Soc. Am. (2001). https://doi.org/10.1785/0120000703.

[31] D. Melgar, Y. Bock, D. Sanchez, B.W. Crowell, On robust and reliable automated baseline corrections for strong motion seismology, J. Geophys. Res. Solid Earth. 118 (2013) 1177–1187. https://doi.org/10.1002/jgrb.50135.

[32] A. Bilich, K.M. Larson, Mapping the GPS multipath environment using the signal-to-noise ratio (SNR), Radio Sci. 42 (2007) 1–16. https://doi.org/10.1029/2007RS003652.

[33] G. Lizurek, Full Moment Tensor Inversion as a Practical Tool in Case of Discrimination of Tectonic and Anthropogenic Seismicity in Poland, Pure Appl. Geophys. 174 (2017) 197–212. https://doi.org/10.1007/s00024-016-1378-9.

[34] P. Xu, Y. Shu, X. Niu, J. Liu, W. Yao, Q. Chen, High-rate multi-GNSS attitude determination: Experiments, comparisons with inertial measurement units and applications of GNSS rotational seismology to the 2011 Tohoku Mw9.0 earthquake, Meas. Sci. Technol. 30 (2019). https://doi.org/10.1088/1361-6501/aaf987.

[35] N. Houlié, D. Dreger, A. Kim, GPS source solution of the 2004 Parkfield earthquake, Sci. Rep. 4 (2014). https://doi.org/10.1038/srep03646.

[36] H. Doležalová, V. Kajzar, K. Souček, L. Staš, Evaluation of mining subsidence using GPS data, Acta Geodyn. Geomater. 6 (2009) 359–367.

[37] R. Dong-feng, L. Yun-peng, M. Zhen-li, Test and analysis on the errors of GPS observation in mining field, Procedia Earth Planet. Sci. 1 (2009) 1233–1236. https://doi.org/10.1016/j.proeps.2009.09.189.

[38] C.H. Xu, J.L. Wang, J.X. Gao, J. Wang, H. Hu, Precise point positioning and its application in mining deformation monitoring, Trans. Nonferrous Met. Soc. China (English Ed. 21 (2011) 499–505. https://doi.org/10.1016/S1003-6326(12)61632-X.

[39] J. Wang, X. Peng, C.H. Xu, Coal mining GPS subsidence monitoring technology and its application, Min. Sci. Technol. 21 (2011) 463–467. https://doi.org/10.1016/j.mstc.2011.06.001.

[40] H.F. Bian, S.B. Zhang, Q.Z. Zhang, N.S. Zheng, Monitoring large-area mining subsidence by GNSS based on IGS stations, Trans. Nonferrous Met. Soc. China (English Ed. 24 (2014) 514–519. https://doi.org/10.1016/S1003-6326(14)63090-9.

[41] H. Fan, X. Gao, J. Yang, K. Deng, Y. Yu, Monitoring mining subsidence using a combination of phase-stacking and offset-tracking methods, Remote Sens. 7 (2015) 9166–9183. https://doi.org/10.3390/rs70709166.

[42] R. Orús, M. Hernández-Pajares, J.M. Juan, J. Sanz, Improvement of global ionospheric VTEC maps by using kriging interpolation technique, J. Atmos. Solar-Terrestrial Phys. 67 (2005) 1598–1609. https://doi.org/10.1016/j.jastp.2005.07.017.

[43] T. Takasu, RTKLIB: Open source program package for RTK-GPS, in: FOSS4G 2009 Tokyo, Japan, Novemb. 2, 2009, 2009. http://www.rtklib.com.

[44] F. Moschas, S. Stiros, Noise characteristics of high-frequency, short-duration GPS records from analysis of identical, collocated instruments, Meas. J. Int. Meas. Confed. 46 (2013) 1488–1506. https://doi.org/10.1016/j.measurement.2012.12.015.

[45] S. Kim, J.P. Stewart, Kinematic soil-structure interaction from strong motion recordings, J. Geotech. Geoenvironmental Eng. 129 (2003) 323–335.

[46] C. Leys, C. Ley, O. Klein, P. Bernard, L. Licata, Detecting outliers: Do not use standard deviation around the mean, use absolute deviation around the median, J. Exp. Soc. Psychol. 49 (2013) 764–766. https://doi.org/10.1016/j.jesp.2013.03.013.

[47] L.Y. Low, P.J. Huber, Robust Statistics., Springer, 1983. https://doi.org/10.2307/2287149.

## 9. Figure captions

Figure 1: Distribution of the high-rate GNSS stations (green circles) and the seismic stations (squares) in the proximity of the 2019 mining tremor. The black star is the epicentre location. The data from the earthquake catalogue refer to the period July 2018 to March 2019.

Figure 2: Fourier spectra of band-pass filtered displacement waveforms.

Figure 3: Coherence values of band-pass filtered displacements calculated with the PPP (top) and DD (bottom) approaches.

Figure 4: Time variability of Pearson's correlation coefficient of band-pass filtered displacements in comparison with seismological data for station KOMR/LES1. Left panel "a" presents 2-minute time series of SM and PPP-displacements. Right panel "b" presents 30-second time series of SM, PPP and DD-displacements. On both panels, the correlation coefficient variability for both solutions is presented.

Figure 5: Time variability of Pearson's correlation coefficient of band-pass filtered displacements in comparison with seismological data on 2-minute time series. Left panel "a" presents PPP-displacements for station TRZB/TRBC and right panel "b" presents DD-displacements for station TARN/TRN2. On both panels, the correlation coefficient variability for both solutions is presented.

Figure 6: Statistics for the station LES1 2-minute band-pass filtered displacement time series calculated with the PPP (right) and DD approaches (left).

Figure 7: Statistics for the LES1 1-hour band-pass filtered displacement time series calculated with the PPP (right) and DD approaches (left).

Figure 8: Statistics for the TRZB 1-hour band-pass filtered displacement time series calculated with the PPP (right) and DD approaches (left).

## 10. Table captions

Table 1: Details of co-located high-rate GNSS and strong-motion stations.

Table 2: Accuracy of non-filtered (linear detrended) and band-pass filtered GPS-positions in stable conditions. The accuracy was determined as the unbiased version of RMSE. The time span is 2 minutes.

Table 3: Peak ground displacements, peak-to-peak amplitudes and RMSE of filtered PPP and DD displacements (mm).

Table 4: List of maximum correlation coefficients for PPP/SM and DD/SM band-pass filtered displacement time series.

***Credit Author Statement***

Iwona Kudłacik – Methodology, Software, Validation, Formal analysis, Investigation, Visualization, Writing - Original Draft

Jan Kapłon – Conceptualization, Investigation, Resources, Writing - Review & Editing, Supervision

Grzegorz Lizurek – Resources, Writing - Review & Editing

Mattia Crespi – Conceptualization, Writing - Review & Editing

Grzegorz Kurpiński – Resources, Writing - Review & Editing

***HIGHLIGHTS***

The mining tremor might be tracked via high-rate GNSS stations.

With high-rate GPS observations, subcentimetre vibrations can be detected.

It is possible to detect a mining tremor with a GPS displacement time series alone.

GNSS-seismology applies to the analysis of anthropogenic seismic activity.